

# Analytical Methods

Accepted Manuscript



This is an *Accepted Manuscript*, which has been through the Royal Society of Chemistry peer review process and has been accepted for publication.

*Accepted Manuscripts* are published online shortly after acceptance, before technical editing, formatting and proof reading. Using this free service, authors can make their results available to the community, in citable form, before we publish the edited article. We will replace this *Accepted Manuscript* with the edited and formatted *Advance Article* as soon as it is available.

You can find more information about *Accepted Manuscripts* in the [Information for Authors](#).

Please note that technical editing may introduce minor changes to the text and/or graphics, which may alter content. The journal's standard [Terms & Conditions](#) and the [Ethical guidelines](#) still apply. In no event shall the Royal Society of Chemistry be held responsible for any errors or omissions in this *Accepted Manuscript* or any consequences arising from the use of any information it contains.

# A XANES study of chromophores: the case of black glass

Andrea Ceglia,<sup>\*a,b,c</sup> Gert Nuyts,<sup>d</sup> Simone Cagno,<sup>d,e</sup> Wendy Meulebroeck,<sup>a</sup> Kitty Baert,<sup>a</sup> Peter Cosyns,<sup>c</sup> Karin Nys,<sup>c</sup> Hugo Thienpont,<sup>b</sup> Koen Janssens,<sup>d</sup> and Herman Terryn<sup>a</sup>

Received Xth XXXXXXXXXXXX 20XX, Accepted Xth XXXXXXXXXXXX 20XX

First published on the web Xth XXXXXXXXXXXX 200X

DOI: 10.1039/b000000x

We studied the Fe K-edge X-ray absorption near edge (XANES) spectra of several Roman black glass fragments in order to determine the  $\text{Fe}^{3+}/\Sigma\text{Fe}$  ratio of these materials. The selected archaeological glass samples cover the period 1<sup>st</sup>-5<sup>th</sup> century AD in nine different sites of the North Western provinces of the Roman Empire. The fragments belong to two different compositional groups demonstrating a diachronic evolution: early Roman HMG (High Magnesia Glass) and Roman Imperial LMG (Low Magnesia Glass). The first group contains natural Fe levels (below 2 wt% as  $\text{Fe}_2\text{O}_3$ ), while the LMG has concentrations above 5 wt%. This difference is also reflected by  $\text{Fe}^{3+}/\Sigma\text{Fe}$  values. Low iron glass was produced under strongly reducing conditions in order to obtain the black colour, with average  $\text{Fe}^{3+}/\Sigma\text{Fe}$  values  $\approx 0.17$ . LMG glass is somewhat more oxidised ( $\text{Fe}^{3+}/\Sigma\text{Fe} \approx 0.4$ -0.5). While HMG glass required active control of the furnace environment, LMG was made under ambient atmosphere and their higher oxidation degree is mainly determined by the chemistry of the raw glass.

## 1 Introduction

Compositional analysis is routinely performed on archaeological glass artefacts.<sup>1</sup> Quantitative compositional data can form the basis for the reconstruction of ancient recipes and may indirectly help unravelling the distribution, trade and consumption of glass in former periods, and in a wider perspective, may provide new data to allow a better understanding of ancient economies. However, this elemental information is not always sufficient to describe all relevant properties of glass. In several historical periods, the colour of glass artefacts has been an important characteristic. Colour in glass is imparted by several transition metals and both the redox state and the coordination geometry of metal ions affect the final hue. Redox conditions in the glass furnace and of the melt are therefore important for determining the final aspect of a glass artefact; hence, an indirect determination of these conditions allows to better understand the skills required for glass making.

In man-made glass, iron is always present because of its natural occurrence in (heavy) minerals associated with sand. By controlling the furnace conditions, or by adding redox-

sensitive elements, glass makers can change the  $\text{Fe}^{3+}/\Sigma\text{Fe}$  ratio and generate hues ranging from brown (in presence of sulphur) over green to blue or optionally may produce colourless glass.

In a recent paper, Arletti et al.<sup>2</sup> studied the Mn K-edge and Fe K-edge X-ray Absorption Near Edge Spectroscopy (XANES) profiles of 15 archaeological glass samples. The fragments investigated were iron-coloured glass of different shades, some glass decolourised by means of manganese or antimony oxides and one example of purple coloured glass. The results of their analysis offered a deeper insight into ancient glassmaking technology.

In this paper, we investigate the redox conditions employed in Roman glass workshops to produce black glass, a particular type of artefact made in the Roman glass industry. Black glass artefacts are a source of relevant historical information. They can be linked to patterns of regional consumption and specific periods.<sup>3</sup> Black glass was mainly employed to produce vessels and jewellery. Black glass jewellery was manufactured throughout the entire Roman imperial period, but became especially common from the second half of the 2<sup>nd</sup> century AD onwards.<sup>3</sup> The production of glass bangles, finger rings, beads, pendants, hairpins and gems disappeared gradually during the 5<sup>th</sup> century AD in the Western part of the Empire.<sup>3</sup>

Black appearing glass vessels were fashionable at three different stages in Roman history. In the first phase of black glass vessel consumption from about 30 to 70-80 AD, these artefacts enjoyed an Empire-wide distribution. The production of black glass vessels was initiated by glass workshops in the South-Eastern Mediterranean where also other deeply

<sup>a</sup> Department of Electrochemical and Surface Engineering, SURF research group, Vrije Universiteit Brussel, Pleinlaan 2, B-1050 Brussels, Belgium. Fax: +32 2 629 3200; Tel: +32 2 629 3534; E-mail: [aceglia@vub.ac.be](mailto:aceglia@vub.ac.be)

<sup>b</sup> Department of Applied Physics and Photonics, Brussels Photonics Team B-PHOT, Vrije Universiteit Brussel, Pleinlaan 2, B-1050 Brussels, Belgium.

<sup>c</sup> Department of Art Sciences and Archaeology, MARI research group, Vrije Universiteit Brussel, Pleinlaan 2, B-1050 Brussels, Belgium.

<sup>d</sup> Department of Chemistry, AXIL research group, Universiteit Antwerpen, Groenenborgerlaan 171, B-2020 Antwerpen, Belgium.

<sup>e</sup> Department Plant and Environmental Sciences, Norwegian University of Life Sciences (UMB), P.O. Box 5003, 1432 Aas, Norway.

coloured monochrome glass vessels were produced. Soon the production moved to new glass workshops in Italy, France and Switzerland. Between 170-180 AD and 230-250 AD, black glass gained again favour within the North Western provinces Gallia Belgica, Germania Inferior and Germania Superior.<sup>3,4</sup> During the 4<sup>th</sup>-5<sup>th</sup> century AD, there was a third re-emergence of this particular glass production, limited however to the South-Eastern Mediterranean.<sup>3</sup>

In previous papers several hundred fragments of black glass were analysed.<sup>3,5-7</sup> The analysed sample set encompassed material from 1<sup>st</sup> to the 5<sup>th</sup> century AD, originating from the entire Roman Empire, i.e. from East to West and from South to North. The colour description “black” generalises the perceived hue because the real colour is not observable due to the high concentration of colouring oxides in the glass matrix. Black glass can be obtained by introducing one or several colouring agents in large abundance. It has been proposed that the regional production and distribution of (black) glass implies a gradual improvement of technological knowledge.<sup>3,7</sup> However, most black glass generated has a deep green hue, using iron as chromophoric element. Among the dark green/black glass, it is possible to distinguish two different recipes: a low iron ( $\text{Fe}_2\text{O}_3 < 2 \text{ wt}\%$ ) and a high iron ( $\text{Fe}_2\text{O}_3 > 5 \text{ wt}\%$ ) soda-lime-silicate glass. The first type could be dated prior to 150 AD and received an Empire-wide distribution, while the second glass type appeared only at the end of the 2<sup>nd</sup> century.<sup>7</sup> Another important difference is that low iron glass is characterised by high magnesium and potassium concentrations, typical of glass made from sand and plant ash. High iron glass has on the contrary the classical Roman low magnesium, low potassium chemical composition, obtained by fusing relatively pure lime-bearing sand and mineral soda,<sup>8</sup> to which, iron was added to impart the colour.<sup>5-7</sup>

The chemical composition obtained by SEM-EDX allows to determine the total iron concentration in the glass. If a glass with a specific amount of iron is produced under different redox conditions, its  $\text{Fe}^{3+}/\Sigma\text{Fe}$  ratio changes accordingly. XANES allows to determine how much of the total iron is in the ferrous ( $\text{Fe}^{2+}$ ) or ferric ( $\text{Fe}^{3+}$ ) state. By systematically determining  $\text{Fe}^{3+}/\Sigma\text{Fe}$  ratio for a series of 27 black appearing glass samples, this study aims to contribute new information on the ancient glass technology. More specifically,  $\text{Fe}^{3+}/\Sigma\text{Fe}$  ratio is considered to be a key parameter permitting to investigate whether redox conditions were intentionally modified in glass furnaces in some periods of the Roman Empire to produce black glass. Besides XANES, we employed Raman spectroscopy in order to probe qualitatively the presence of the  $\text{Fe}^{3+}\text{-S}^{2-}$  complex. The resonant effect allows to detect ppm levels of the complex.<sup>9,10</sup> This specie absorbs very strongly in the visible region, hence, its presence might contribute to the formation of black color. Furthermore, this chromophore is a marker of particularly reducing conditions as it starts forming

when  $\text{Fe}^{3+}/\Sigma\text{Fe}$  decreases below 0.50.<sup>11</sup>

## 2 Experimental section

### 2.1 The archaeological glass

All the glass fragments analysed belong to the so-called black appearing glass. We selected 27 samples taken from vessels and jewellery dating between the 1<sup>st</sup> and the 5<sup>th</sup> century AD and originating from nine Western European archaeological sites. All sampled fragments come from consumption sites. Nevertheless, the samples from Augst (Switzerland) and Trier (Germany) might have been produced in their respective local glass workshops.<sup>3</sup> In Table 1 we report the chemical composition obtained by SEM-EDX, period of production, place of excavation and type of artefact.<sup>5</sup>

While all the selected fragments are black appearing green glasses with a soda lime glass base composition (with the  $\text{Na}_2\text{O}$  concentration between 14.7 and 20.9 wt%), they belong to three different chemical groups. A first group consists of 11 samples of High Magnesia Glass (HMG)<sup>8</sup> dated to the 1<sup>st</sup> and up to the mid 2<sup>nd</sup> century AD. These glasses were made using iron-containing sand and plant ash and no intentional addition of iron took place.<sup>5</sup> The second large group is Low Magnesia Glass (LMG)<sup>8</sup>, obtained by using sand and mineral soda and dated between the 2<sup>nd</sup> and the 4<sup>th</sup> century AD. This compositional group consists of 14 glass fragments to which iron was deliberately added in order to obtain the black aspect. We report here also the data obtained on two samples from a 4<sup>th</sup>-5<sup>th</sup> century context, excavated in Trier having a High Iron, Manganese and Titanium (HIMT) glass composition.<sup>12</sup> Also in these two glasses, iron was deliberately added to achieve the black appearance. Although two samples are limited and no conclusions on this group will be drawn, these samples are relevant a reference for future studies on HIMT glass.

### 2.2 X-ray Absorption Near Edge Spectroscopy (XANES)

The Fe-K edge XANES measurements were performed at DORIS III, Beamline L, Hamburg (Germany). A Si(111) double crystal monochromator was used, having an energy resolution  $\Delta E/E$  of about  $10^{-4}$ . A transmission XANES spectrum was recorded from a metallic Fe reference foil (7.5  $\mu\text{m}$ ) and used to provide an accurate energy calibration for all spectra; the first inflection point of the Fe-K edge was set to 7112 eV.<sup>13</sup> A slight detuning of the two monochromator crystals was used to remove the high energy harmonics from the incident X-ray beam. The reference compounds  $\text{FeCl}_3$  and  $\text{FeSO}_4$  provided reference spectra for ferrous and ferric iron. In order to limit self-absorption, these powdered compounds were diluted to  $\pm 2\%$  with cellulose and pressed into a pellet. To avoid contributions of possible heterogeneities during mixing, the

reference XANES spectra were recorded with an unfocused beam. Next to these reference compounds, also two soda-lime-silicate glasses, ST1 and ST2 were analysed. The two glasses contain a different total amount of iron (0.1 wt% and 0.6 wt% as  $\text{Fe}_2\text{O}_3$  respectively) but have an identical  $\text{Fe}^{3+}/\Sigma\text{Fe}$  ratio estimated to be equal to 0.67.<sup>2,14</sup> XANES spectra were recorded with the sample oriented at  $45^\circ$  to the incoming beam. The fluorescence yield was collected using a Vortex silicon drift chamber detector at an angle of  $45^\circ$  with respect to the sample surface. ROI (Region Of Interest) fitting around the  $\text{FeK}_\alpha$  line (6113-6692 eV) was performed. XANES spectra were collected from  $\sim 32$  eV below to  $\sim 130$  eV above the Fe-K edge using different energy intervals (7090 eV - 7105 eV: 0.25 eV, 7105 eV - 7120 eV: 0.1 eV, 7120 eV - 7250 eV: 0.25 eV); a measuring time of 1 s was used for each energy step resulting in a  $\sim 20$  min measuring time per XANES spectrum. Three repeats were recorded for each Fe model compound in order to acquire virtually noise-free spectra. The measurements of the historical glass fragments discussed in this article were performed under the same conditions as the reference compounds. The size of the focused primary beam was made as large as possible, circa  $780 \times 520 \mu\text{m}^2$ , in order to minimise the influence of possible heterogeneities in the analysed glass fragments. A polycapillary lens was used for focusing but the sample surface was at a larger distance than the focal length of the lens. All scans were recorded on the bulk of the samples. The thickness of the embedded samples (several mm) prevented transmission XANES measurements, thus allowing only monitoring of the fluorescence intensity as a function of the excitation energy. For all XANES spectra, the normalisation was performed by means of the software package ATHENA. An edge-step normalisation was performed by a linear pre-edge subtraction and by regression of an (in general) third degree polynomial beyond the edge.<sup>15</sup>

The pre-edge peak is extracted using an arctangent function to describe the background. In literature different functions have been employed for the description of the pre-edge features.<sup>16</sup> When the same mathematical model is used throughout the entire data set, the conclusions will be consistent. Problems may arise when comparing the data to literature values.<sup>17</sup> For the glass samples, the Fe-K pre-edge features have been fitted using two Voigt peaks with 2 eV of average width.<sup>16-20</sup> For the reference compounds, it was necessary to include a third peak function to obtain good fits. All peaks were constrained to have a 50% Lorentzian-50% Gaussian shape.

### 2.3 Raman spectroscopy

Raman spectra are recorded between  $100 \text{ cm}^{-1}$  and  $1300 \text{ cm}^{-1}$  using a LabRam Raman spectrometer (Horiba Jobin Yvon S.A.S, France) equipped with an integrated Olympus

BX40 microscope and a solid state laser emitting at 532 nm.

The data are corrected for the dependence of the scattered intensity on the temperature and frequency using the established method developed by Long.<sup>21-24</sup> All spectra are baseline subtracted using a cubic spline function through data points at  $\sim 200$ ,  $\sim 850$  and  $\sim 1200 \text{ cm}^{-1}$ .

## 3 Results

Figure 1 shows the XANES profiles and the pre-edge absorption features of  $\text{FeSO}_4$ ,  $\text{FeCl}_3$  and ST2, corresponding to  $\text{Fe}^{3+}/\Sigma\text{Fe}$  ratio values of respectively 0.00, 1.00 and 0.67. The position of the absorption edge around 7122 eV is clearly shifting towards higher energy when the  $\text{Fe}^{3+}/\Sigma\text{Fe}$  ratio changes from 0.00 over 0.67 to 1.00. The pre-edge peak located at about 7114 eV behaves accordingly.

The pre-edge features in Fe-K edge XANES spectra are due to  $1s \rightarrow 3d$  transitions.<sup>25</sup> It is well known that the pre-edge features are strongly affected by the oxidation state and the coordination chemistry of the absorbing ion. The higher the oxidation state the higher the energy required for the absorbing transition to occur.<sup>16,17,19,25-27</sup> The centroid of the pre-edge (i.e. the energy position at which half of the total area is integrated) for a determined oxidation state always occurs at the same position irrespective of the coordination geometry. On the other hand, the Fe coordination type has a major effect on the intensity of the pre-edge features, which increase in intensity while changing from 6-fold to 4-fold coordination.<sup>16,25,26</sup> In glass, both the ferrous and the ferric iron can have 4-fold, 5-fold and 6-fold coordination. The extracted pre-edge spectra exhibit a systematic shift of the energy to higher values as the relative abundance of the ferric components increases.

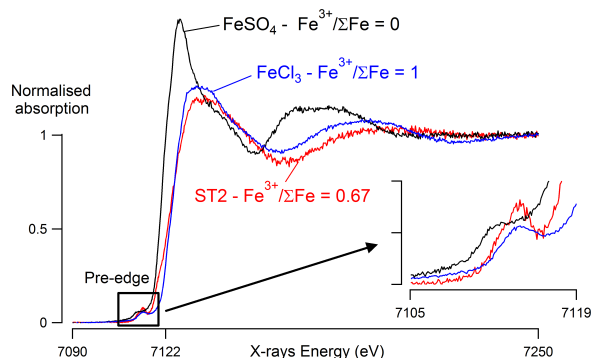


**Fig. 1** Normalised XANES spectra of the reference compounds  $\text{FeSO}_4$ ,  $\text{FeCl}_3$  and glass ST2 show an evident shift of the absorption edge. In the inset, the influence of  $\text{Fe}^{3+}/\Sigma\text{Fe}$  on the  $1s \rightarrow 3d$  pre-edge transition is highlighted

Table 2 reports the fit results of the Fe pre-edges for all black glass samples and reference compounds. The average

positions of the two Voigt functions used to fit the pre-edge peaks of the glass samples are  $7112.4 \pm 0.2$  eV and  $7114.0 \pm 0.2$  eV. The two components are separated by about 1.5 eV in accordance with published data on silicate glasses.<sup>2,16,17</sup>

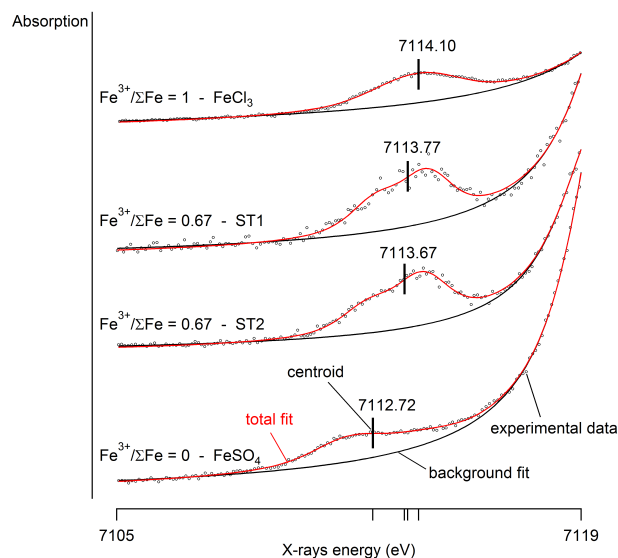


**Fig. 2** Pre-edge absorption of standard glasses ST1, ST2 and reference compounds  $\text{FeSO}_4$  and  $\text{FeCl}_3$ . The centroid position varies from 7112.72 eV for ferrous iron ( $\text{FeSO}_4$ ) to 7114.10 eV for ferric iron ( $\text{FeCl}_3$ )

Figure 2 shows the fits of background and pre-edge for the reference compounds,  $\text{FeSO}_4$  and  $\text{FeCl}_3$ , and for the standard glasses ST1 and ST2. The position of the centroid varies from 7112.72 for ferrous ( $\text{FeSO}_4$ ) to 7114.10 eV ferric iron ( $\text{FeCl}_3$ ).

Although the calibration data set only contains 4 points, it is possible to establish a correlation line that allows to estimate the  $\text{Fe}^{3+}/\Sigma\text{Fe}$  ratio of glass samples.<sup>17</sup> The linear fit and its parameters are reported in Figure 3. For comparison we show also the data obtained by Arletti et al.<sup>2</sup> for almandine ( $\text{Fe}^{2+}$ ), hercynite ( $\text{Fe}^{2+}$ ), ST1 ( $\text{Fe}^{3+}/\Sigma\text{Fe} = 0.67$ ), silicalite ( $\text{Fe}^{3+}$ ). Nevertheless, we computed the linear correlation using only our data. The values of the  $\text{Fe}^{3+}/\Sigma\text{Fe}$  ratio obtained are reported in the last column of Table 2. HMG glass on average features  $\text{Fe}^{3+}/\Sigma\text{Fe} = 0.17 \pm 0.07$ . LMG glass show more disperse values with an average  $\text{Fe}^{3+}/\Sigma\text{Fe}$  ratio of  $0.40 \pm 0.14$ . The two HMT fragments have different values: sample PC13.4 appears fairly oxidised with a  $\text{Fe}^{3+}/\Sigma\text{Fe}$  value of 0.80, while PC13.5 is more reduced, having only 50% of iron in the ferric state.

Figure 4 shows the extrapolated pre-edge features of three Roman black glasses in comparison to standard glass ST2. The evolution of the pre-edge peak positions reflects well the change in oxidation state.

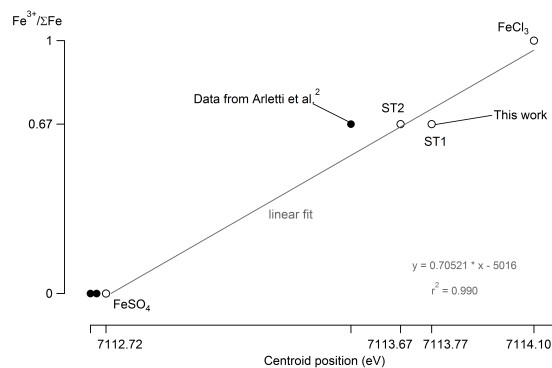


**Fig. 3** The centroid position of the standard glasses ST1 and ST2 and reference compounds  $\text{FeSO}_4$  and  $\text{FeCl}_3$  are correlated to the  $\text{Fe}^{3+}/\Sigma\text{Fe}$  values. This relationship is used to calculate the ferric fraction in the glass samples

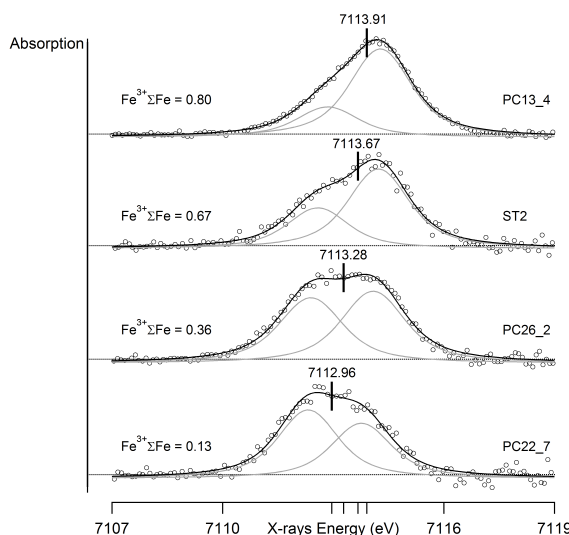


**Fig. 4** Pre-edges X-rays absorption changes systematically with  $\text{Fe}^{3+}/\Sigma\text{Fe}$ . The raw data, the two Voigt peaks used for the fitting and the total fit are superimposed to show the quality of the fits from which the centroid values were determined

## 4 Discussion

### 4.1 Causes and effects of $\text{Fe}^{3+}/\Sigma\text{Fe}$ in glass

Contrasting the usually unintentional presence of iron in the glass batch, iron was the main colourant employed to make black appearing glass. Hence, ancient glassmakers must have known the effect of this metal ion on the final hue of glass. Figure 5 is a scheme of the main parameters affecting  $\text{Fe}^{3+}/\Sigma\text{Fe}$  and the effect of the redox equilibrium on the final glass colour. Different redox ratios yield a large spectrum of

hues.

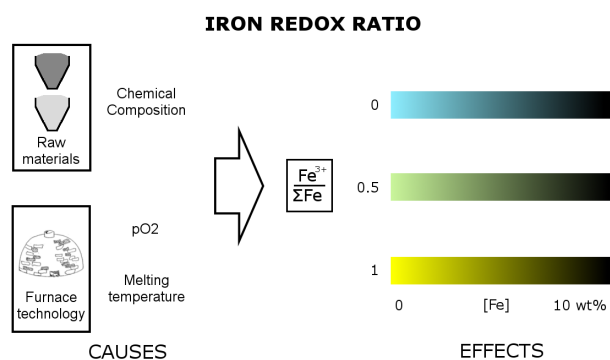


**Fig. 5** Glass batch composition,  $pO_2$  in the furnace and melting temperature affect  $Fe^{3+}/\Sigma Fe$  in glass. This influences the final hue, which is also function of the total iron concentration

In oxidising environments  $Fe^{3+}/\Sigma Fe$  tends to 1 and the colour of glass is pale yellow. The origin of the colour is due to the weak  $d-d$  forbidden transitions of  $Fe^{3+}$  in the region between 380-440 nm and the strong charge-transfer UV absorption which tails in the visible.<sup>11</sup>

Reducing conditions favour the formation of ferrous iron which absorbs strongly in the near infra-red region ( $\sim 1000$  nm in octahedral and  $\sim 2000$  nm in tetrahedral coordination). The absorption band of octahedral  $Fe^{2+}$  tails in the visible electromagnetic spectrum shifting the colour towards blue.<sup>11</sup> Similarly to  $Fe^{3+}$ , ferrous ions absorb in the UV, but at higher energies.<sup>28,29</sup> The coexistence of the two ion species yields a green hue in different shades according to the relative proportion.

In ancient glass small quantities of sulphur are always present as it is introduced as impurity of the fluxes. Under strongly reducing melting conditions,  $S^{2-}/S^{6+}$  equilibrium is moved in favour of the anion. As a consequence, the colour is strongly modified by the formation of the ferri-sulphide complex,  $Fe^{3+}-S^{2-}$ .<sup>30</sup> Despite most of the iron is transformed in  $Fe^{2+}$ , the remaining amount of ferric ions can react with the sulphur present in the batch.  $Fe^{3+}-S^{2-}$  is a strong chromophore which absorbs light due to the presence of a very strong charge-transfer band at 415 nm originating the amber colouration typical of nowadays beer bottles.<sup>31</sup>

Yellow, green, blue or olive hues are some of the possible combinations of the ferric and ferrous ions. The colour is further deepened by the concentration of iron (see Figure 5) or the thickness of the artefact. If the total concentration of iron is high (or the artefact is thick), the combined effect of  $Fe^{2+}$ ,  $Fe^{3+}$  and  $Fe^{3+}-S^{2-}$  results in black appearing glass.

The final redox ratio of iron is the result of the combination of several parameters linked to the chemical composition of raw materials and the furnace technology (Figure 5).

The choice of raw materials, or in other words the glass matrix, influences strongly the redox ratio. Certain compounds affect the redox number of the glass batch.<sup>32,33</sup> Anthracite, carbon, pyrite, sulphides have a reducing effect; while alkali nitrate, sulphates, iron oxide ( $Fe_2O_3$ ) have an oxidising effect.<sup>32,33</sup> A parameter which is related to the glass chemistry is the optical basicity, which is function of the concentration of alkalis (Li, Na, K ...). Optical basicity enhances oxidising conditions and since network modifiers promote glass basicity, glasses with a higher soda content tend to be more oxidised.<sup>34,35</sup> Glass composition is also responsible for possible electrochemical reactions within the glass melt.<sup>36</sup> Antimony and manganese oxides were regularly added to the batch in order to oxidise iron and produce colourless (or weakly coloured) glass.<sup>37</sup>

Besides the raw materials the final  $Fe^{3+}/\Sigma Fe$  values are influenced by furnace technology. The two main parameters are the oxygen partial pressure ( $pO_2$ ) and temperature. Reasonably,  $pO_2$  is linearly correlated to  $Fe^{3+}/\Sigma Fe$ ; hence, pumping air into the glass furnace favours oxidation ( $pO_2$  of air is ca.  $10^{-0.7}$  atm), while a smoky  $CO/CO_2$  rich atmosphere ( $pO_2 \approx 10^{-6}-10^{-12}$  atm) shifts  $Fe^{2+}/Fe^{3+}$  equilibrium towards the reduced state. Concerning the temperature, ancient furnaces were capable of reaching 1100-1200 °C.<sup>28,30,38-40</sup> For a given soda-lime-silicate system, increasing the melting temperature promotes the formation of  $Fe^{2+}$ .<sup>41-43</sup>

When the melting temperature is low and the amount of alkali is high, ancient glass should be oxidised. On the other hand, typical Roman glass is partially reduced having a typical blue-green hue. Arletti et al.<sup>2</sup> found that "naturally" coloured Roman glass has equally distributed ferrous and ferric ions. Glass in the secondary workshop of Basinghall, London, presents a  $Fe^{3+}/\Sigma Fe$  value equal to 0.5, while glass from Bet Eliezer, from primary tank furnaces in Israel, shows variable  $Fe^{3+}/\Sigma Fe$  values ranging from 46% to 70%. Accordingly, Brill<sup>30</sup> reports  $Fe^{3+}/\Sigma Fe$  values of 45% for blue-green Roman glass from Jalame. Such reducing conditions were likely due to little ventilation within the chamber which prevented a correct oxygenation of the melt, sensibly lowering the  $pO_2$ , which generate a  $Fe^{3+}/\Sigma Fe$  of about 0.50.

## 4.2 HMG glass - I-III century AD

The  $Fe^{3+}/\Sigma Fe$  values for the black glass samples (Figure 6 and Table 2) show that this hue generally was produced under reducing conditions. Low iron HMG glass, distributed in Western Europe in the 1<sup>st</sup> century AD up to the mid 2<sup>nd</sup> century AD, is strongly reduced with  $Fe^{3+}/\Sigma Fe$  values ranging from 8 to 30%. Literature data<sup>2,30</sup> showed that the average Roman furnace conditions result in about 50% of iron being present in the ferric state. Hence, the values registered for early Roman HMG glass are due to an intentional modification of the redox

conditions.

Within this group, the variability of the  $\text{Fe}^{3+}/\Sigma\text{Fe}$  values appears correlated to the site of production. Glass fragments from Avenches and from Magdalensberg are more reduced than the sampled glasses from London, which have around 25% of ferric ions. This differentiation can be explained by considering the glass chemistry and the technology of ancient glassmaking. It is unlikely that  $p\text{O}_2$  was intentionally changed. The only modification of the environment that glassmakers could make was to use fresh wood to heat the melting chamber. In this way CO and  $\text{CO}_2$  were released in the furnace atmosphere lowering  $p\text{O}_2$ .<sup>44</sup> It is more plausible that they added certain chemical products to reduce the redox number of the batch. Most likely, similarly to modern industry, they were adding carbon to achieve this effect. Such conditions change  $\text{Fe}^{3+}/\Sigma\text{Fe}$  virtually to 0. Nonetheless, the other components of the batch still play an important role on the final redox conditions. An increase of soda favours the formation of ferric ions. Figure 7 shows the relation between  $\text{Fe}^{3+}/\Sigma\text{Fe}$  and  $\text{Na}_2\text{O}$  content for HMG and LMG glass. The early Roman HMG group exhibits a linear correlation. The artefacts from Avenches with the lowest amount of  $\text{Na}_2\text{O}$ , correspond to the samples with the lowest amount of  $\text{Fe}^{3+}$ . Contrary, the fragments from London have the highest  $\text{Na}_2\text{O}$  concentration ( $\approx 20$  wt%), which explains the higher  $\text{Fe}^{3+}/\Sigma\text{Fe}$  values found for these samples.

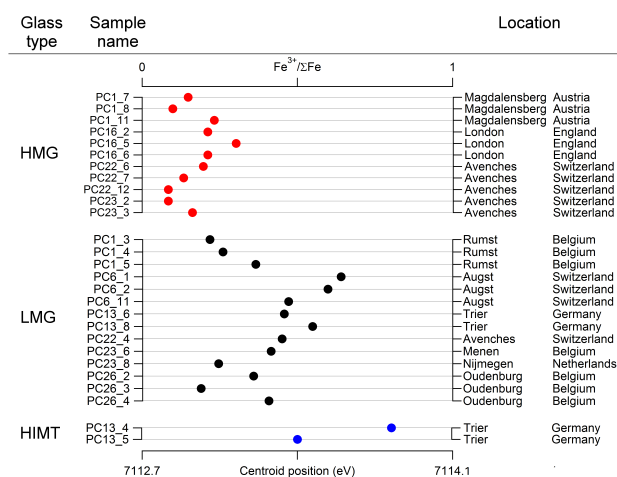


**Fig. 6**  $\text{Fe}^{3+}/\Sigma\text{Fe}$  and centroid position are displayed for all glasses analysed. HMG black glass was obtained by applying strongly reducing conditions, taking advantage of iron impurities in the sand, while LMG and HIMT glass were made black adding large amounts of iron. By doing so, redox conditions no longer played a crucial role

The origin of the black colour of these fragments is due to strongly reducing conditions. The amount of iron alone can not explain the black colour of the glass (Table 2). However, at these reducing conditions the  $\text{Fe}^{3+}-\text{S}^{2-}$  complex can form. Its

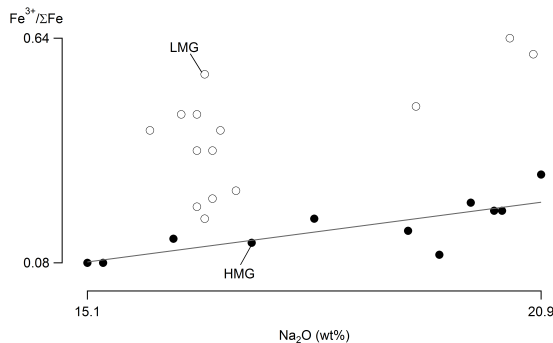


**Fig. 7** In HMG glass  $\text{Fe}^{3+}/\Sigma\text{Fe}$  and  $\text{Na}_2\text{O}$  are linearly correlated, while LMG glass does not have a clear relationship with soda content

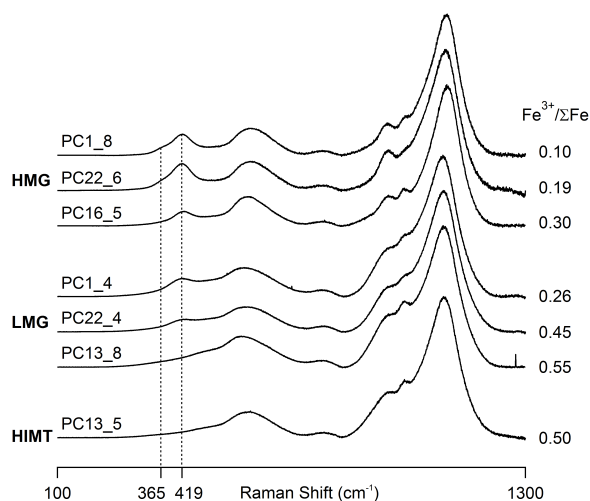


**Fig. 8**  $\text{Fe}^{3+}-\text{S}^{2-}$  complex has a strong Raman signal at  $419\text{ cm}^{-1}$ . When it is present in high concentration a second peak appears as a shoulder at  $365\text{ cm}^{-1}$ . When  $\text{Fe}^{3+}/\Sigma\text{Fe}$  decreases below 0.50, the chromophore starts forming, but its maximum development occurs when  $0.10 < \text{Fe}^{3+}/\Sigma\text{Fe} < 0.30$

presence is confirmed by Raman spectroscopy measurements. All glasses belonging to this group show a typical intense band at  $419\text{ cm}^{-1}$  (see Figure 8). The relatively high amount of chromophore causes a shoulder at  $365\text{ cm}^{-1}$ .<sup>10</sup>

From these observations it is clear that early Roman black glass was produced by intentional application of reducing conditions. This was likely achieved by adding carbon to the batch, probably together with firing fresh wood to run the furnace. Nevertheless, it is not possible at the moment to draw conclusions on when exactly, during the production process, HMG glass was given its black appearance. Two equally plausible options can be considered: 1) black glass was produced

under reducing conditions in primary glass factories and sold as such to secondary workshops, where it was remelted to produce finished objects;<sup>3-5</sup> or 2) glassmakers of secondary workshops bought “naturally” coloured glass and remelted it under reducing conditions to turn it black.

### 4.3 LMG glass - III-V century AD

After the second half of the 2<sup>nd</sup> century a technological change occurred. In continental secondary workshops, rather than applying strongly reducing conditions, glassmakers added large quantities of iron to “naturally” coloured as well as de-colourised glass imported from South East Mediterranean regions.<sup>4</sup> In this manner they could turn the resulting glass black without requiring to explicitly control the redox conditions in the furnace. High iron LMG glass has  $\text{Fe}^{3+}/\Sigma\text{Fe}$  values ranging from 22% and 64%.

Soda content of these fragments does not fully explain the variability of  $\text{Fe}^{3+}/\Sigma\text{Fe}$  within the data set (see Figure 7). The samples from Augst present the highest values of  $\text{Fe}^{3+}/\Sigma\text{Fe}$  together with a relatively high soda content ( $\approx 20$  wt%). On the other hand, all the other glasses have a similar soda content ( $\approx 16-17$  wt%) and their  $\text{Fe}^{3+}/\Sigma\text{Fe}$  values spread between 22% and 55% of ferric ions.

Samples from Rumst, Nijmegen and Oudenburg are the most reduced with  $\text{Fe}^{3+}/\Sigma\text{Fe}$  below 40%. While, the other samples analysed have between 40% and 63% of iron in ferric state. Such values are comparable to what Arletti et al.<sup>2</sup> found for naturally coloured glass from the secondary workshop in Basinghall (London) and the primary glass furnace of Bet Eliezer (Israel). This suggests that in this archaeological sites redox conditions were not intentionally modified. Nevertheless, it should be borne in mind that the variability of  $\text{Fe}^{3+}/\Sigma\text{Fe}$  might be due to different sources of iron. As stated above, pyrite would have a reducing effect while haematite an oxidising one.

The black colour of these fragments is due to the high amount of iron used to fabricate them. The presence of both ions in the glass reduce the transmission of light, making the artefacts appear black. Raman spectroscopy shows that the ferri-sulphide complex is again present in many of the samples (see Figure 8). The more reduced samples have a more intense band of the  $\text{Fe}^{3+}-\text{S}^{2-}$  complex, which disappears for samples with  $\text{Fe}^{3+}/\Sigma\text{Fe} > 0.50$ . Normally, this chromophore starts forming when  $\text{Fe}^{3+}/\Sigma\text{Fe}$  is below 50% and it reaches its thermodynamic optimum when  $\text{Fe}^{3+}/\Sigma\text{Fe}$  ranges between 10% and 30%.<sup>11</sup>

### 4.4 HIMT glass - IV-V century AD

Only two glass samples are made of HIMT glass, produced after the second half of the 4<sup>th</sup> century. In both cases iron

was added intentionally to a HIMT base glass imported from primary factories likely located in Egypt. Seeing the limited amount of samples, we present the data without further discussion as a reference for further studies. Both glass samples stand out among the other analysed samples because of their high Mn content (1.4 and 1.8 wt% when expressed as  $\text{MnO}$ ). It is widely known that pyrolusite ( $\text{MnO}_2$ ) is used as oxidation agent for iron.<sup>1</sup> Because of its high manganese content, naturally coloured HIMT glass is generally rather oxidised, with at least 80% of the iron present in the ferric form.<sup>2,45</sup> The two glass samples originate both from an archaeological site in Trier, Germany. Yet, they have a rather different composition. PC13.4 is the most oxidised glass ( $\text{Fe}^{3+}/\Sigma\text{Fe} = 0.82$ ) of the full samples set, while PC13.5 features a  $\text{Fe}^{3+}/\Sigma\text{Fe}$  value of only 0.50.

Similarly to LMG glass, the black appearance of HIMT fragments is linked to the high amount of iron employed to make this glass.

## 5 Conclusions

Fe K-edge XANES spectroscopy of glass is a useful source of information, allowing to characterise the redox conditions employed by ancient glassmakers. The iron XANES data are complementary to elemental compositional information. Although techniques such as SEM-EDX, XRF or EPMA provide the base chemistry of the glass matrix, they do not distinguish among the contributions of the ferrous and ferric iron, which is a relevant parameter testifying to the redox conditions during the production of coloured glass.

At first, black appearing glass artefacts were made by remelting raw glass without addition of specific colouring agents. The colouring process may have been performed either in the primary or in the secondary glass workshops. In both cases the making of black appearing glass with a relatively low iron content required skilled glassmakers who were able to control the redox environment in the furnace and were aware of its effects. Since in primary workshops, we can assume a more profound knowledge of glass chemistry to have been present, it is more likely to assume that also the colouring process and the use of reducing conditions took place here. Strongly reducing conditions favour the formation of highly absorbing colour centres due to the presence of ferrous iron ions. The latter shift the UV-absorption spectrum of the glass into the visible part of the electromagnetic spectrum and, if sulphur is present, foster the development of the ferri-sulphide complex.

After the second half of the 2<sup>nd</sup> century AD a different and technologically more simple procedure was adopted to produce black glass. Large quantities of iron were added to turn glass black without requiring specific control of the redox conditions in the furnace. The main advantage of this

alternative procedure was that the level of required fuel and of glassmaking skills was significantly lower than before. Its improved cost-effectiveness probably contributed to its economic success. The  $\text{Fe}^{3+}/\Sigma\text{Fe}$  values for the 2<sup>nd</sup> century AD glasses is similar to what Arletti et al.<sup>2</sup> found for naturally coloured glass. This supports the hypothesis that the furnace conditions were not explicitly controlled and that this range of  $\text{Fe}^{3+}/\Sigma\text{Fe}$  values were achieved under uncontrolled kiln conditions. In view of the more simple procedure employed for colouring of high iron glasses, it appears plausible that this effect was obtained in secondary workshops, where “naturally” coloured or decolourised raw glass was remelted and given the black hue. However, LMG glass from the sites of Rumst, Nijmegen and Oudenburg was made coupling both characteristics: high iron concentration and strongly reducing conditions. It is possible that in these areas the new and the old technologies were mixed or that glassmakers used a specific iron ore which would lower the redox conditions of the glass batch (i.e.  $\text{FeS}_2$ ).

## 6 Acknowledgement

The authors are grateful to the staff of beamline L in HASY-LAB for their helpful support. The research leading to these results has received funding from the European Union Seventh Framework Programme FP7/2007-2013 under grant agreement n° 265010. Support from the University of Antwerp Research Council through GOA Programme “XANES meets ELNES” is gratefully acknowledged. We would like to thank M.P. Riccardi and E. Basso of the University of Pavia and R. Falcone of the Stazione Sperimentale del Vetro who provided us with the reference glasses.

## References

- 1 Janssens, *Modern Methods for Analysing Archaeological and Historical Glass*, Wiley, Antwerp, Belgium, 2013.
- 2 R. Arletti, S. Quartieri and I. C. Freestone, *Applied Physics A*, 2012, **111**, 99–108.
- 3 P. Cosyns, *PhD*, Vrije Universiteit Brussels, 2011.
- 4 P. Cosyns and F. Hanut, *Annales of the 16th AIHV Congress*, Nottingham, 2005, pp. 113–118.
- 5 S. Cagno, *PhD*, University of Antwerp, 2012.
- 6 S. Cagno, P. Cosyns, A. Izmer, F. Vanhaecke, K. Nys and K. Janssens, *Journal of Archaeological Science*, 2013, **Submitted**, year.
- 7 V. Van Der Linden, P. Cosyns, O. Schalm, S. Cagno, K. Nys, K. Janssens, A. Nowak, B. Wagner and E. Bulska, *Archaeometry*, 2009, **51**, 822–844.
- 8 E. V. Sayre and R. W. Smith, *Science (New York, N.Y.)*, 1961, **133**, 1824–6.
- 9 L. C. Prinsloo and P. Colomban, *Journal of Raman Spectroscopy*, 2008, **39**, 79–90.
- 10 L. C. Prinsloo, A. Tournié and P. Colomban, *Journal of Archaeological Science*, 2011, **38**, 3264–3277.
- 11 C. R. Bamford, *Colour generation and control in glass*, Elsevier, Amsterdam, 1977, p. 224.
- 12 I. C. Freestone, *Excavations at Carthage*, Oxford University Press, 1994, vol. II, ch. Appendix, p. 290.
- 13 W. H. McMaster, N. Kerr Del Grande, J. H. Mallett and J. H. Hubbell, *Compilation of X-Ray Cross Sections*, Laboratory Lawrence Radiation UCRL-50174 Report National Bureau of Standards, Springfield, VA, 1969.
- 14 S. Quartieri, M. P. Riccardi, B. Messiga and F. Boscherini, *Journal of Non-Crystalline Solids*, 2005, **351**, 3013–3022.
- 15 B. Ravel and M. Newville, *Journal of synchrotron radiation*, 2005, **12**, 537–41.
- 16 F. Farges, Y. Lefrère, S. Rossano, A. Berthereau, G. Calas and G. E. Brown Jr, *Journal of Non-Crystalline Solids*, 2004, **344**, 176–188.
- 17 A. J. Berry, H. S. C. O'Neill, K. D. Jayasuriya, S. J. Campbell and G. J. Foran, *American Mineralogist*, 2003, **88**, 967–977.
- 18 A. J. Berry, L. V. Danyushevsky, H. S. C. O'Neill, M. Newville and S. R. Sutton, *Nature*, 2008, **455**, 960–963.
- 19 G. Giuli, E. Paris, G. Pratesi, C. Koeberl and C. Cipriani, *Meteoritics & Planetary Science*, 2003, **1186**, 1181–1186.
- 20 G. Giuli, S. G. Eeckhout, C. Koeberl, G. Pratesi and E. Paris, *Meteoritics & Planetary Science*, 2008, **986**, 981–986.
- 21 D. A. Long, *Raman spectroscopy*, McGraw-Hill, New York, 1977.
- 22 B. O. Mysen and L. Finger, *American Mineralogist*, 1982, **67**, 686–695.
- 23 B. Cochain, D. R. Neuville, G. S. Henderson, C. A. McCammon, O. Pinet and P. Richet, *Journal of the American Ceramic Society*, 2012, **95**, 962–971.
- 24 A. Di Muro, N. Métrich, M. Mercier, D. Giordano, D. Massare and G. Montagnac, *Chemical Geology*, 2009, **259**, 78–88.
- 25 M. Wilke, F. Farges and P. E. Petit, *American Mineralogist*, 2001, **86**, 714–730.
- 26 T. E. Westre, P. Kennepohl, J. G. DeWitt, B. Hedman, K. O. Hodgson and E. I. Solomon, *Journal of the American Chemical Society*, 1997, **119**, 6297–6314.
- 27 M. Abuín, A. Serrano, J. Chaboy, M. A. García and N. Carmona, *Journal of Analytical Atomic Spectrometry*, 2013, **28**, 1118.
- 28 P. A. Bingham and C. M. Jackson, *Journal of Archaeological Science*, 2008, **35**, 302–309.
- 29 T. T. Volontinen, J. M. Parker and P. A. Bingham, *Physics and Chemistry of Glasses: European Journal of Glass Science and Technology Part B*, 2008, **49**, 258–270.
- 30 R. H. Brill, *Excavations at Jalame: site of a glass factory in late Roman Palestine*, University of Missouri, Columbia, 1988, ch. 9, pp. 257–294.
- 31 J. W. H. Schreurs and R. H. Brill, *Archaeometry*, 1984, **26**, 199–209.
- 32 W. Simpson and D. Myers, *Glass Technology*, 1978, **19**, 82–85.
- 33 N. F. Zhernovaya, N. I. Minko, V. I. Onishchuk and L. I. Melnikova, *Glass and Ceramics*, 2000, **57**, 84–86.
- 34 W. Thiemson, K. Keowkammer, S. Phanichphant, P. Suwannathada and H. Hessenkemper, *Glass Physics and Chemistry*, 2008, **34**, 19–29.
- 35 J. Duffy, *Journal of Non-Crystalline Solids*, 1996, **196**, 45–50.
- 36 H. D. Schreiber, B. K. Kochanowski, C. W. Schreiber, A. B. Morgan, M. Coolbaugh and T. G. Dunlap, *Journal of Non-Crystalline Solids*, 1994, **177**, 340–346.
- 37 C. M. Jackson, *Archaeometry*, 2005, **47**, 763–780.
- 38 C. M. Jackson, P. T. Nicholson and W. Gneisinger, *Journal of Glass Studies*, 1998, **40**, 11–23.
- 39 C. M. Jackson, L. Joyner, C. A. Booth, P. M. Day, E. C. W. Wager and V. Kilikoglou, *Archaeometry*, 2003, **45**, 435–456.
- 40 P. T. Nicholson and C. M. Jackson, *Brilliant things for Akhenaten: the production of glass, vitreous materials and pottery at Amarna Site O45.1 (EES Excavation Memoir 80)*, Egypt Exploration Society, London, 2007, ch. 4, pp. 83–100.
- 41 B. Mirhadi and B. Mehdikhani, *Journal of the Korean Ceramic Society*, 2011, **48**, 117–120.

- 
- 1  
2  
3 42 E. S. Dunaeva, E. Brunet, S. Muller and I. A. Uspenskaya, *Russian Journal of Inorganic Chemistry*, 2012, **57**, 1355–1361.  
4  
5 43 R. K. Kukkadapu, H. Li, G. L. Smith, J. D. Crum, J.-S. Jeoung, W. H. Poisl and M. C. Weinberg, *Journal of Non-Crystalline Solids*, 2003, **317**, 301–318.  
6  
7 44 P. A. Bingham, J. M. Parker, T. M. Searle and I. Smith, *Journal of Non-Crystalline Solids*, 2007, **353**, 2479–2494.  
8  
9 45 L. De Ferri, R. Arletti, G. Ponterini and S. Quartieri, *European Journal of Mineralogy*, 2011, **23**, 969–980.  
10  
11  
12  
13  
14  
15  
16  
17  
18  
19  
20  
21  
22  
23  
24  
25  
26  
27  
28  
29  
30  
31  
32  
33  
34  
35  
36  
37  
38  
39  
40  
41  
42  
43  
44  
45  
46  
47  
48  
49  
50  
51  
52  
53  
54  
55  
56  
57

**Table 1** List of the samples analysed by SEM-EDX. The table indicates also object type, century and site of excavation (after Cagno<sup>5</sup>).

<sup>a</sup> Au: Augst (Switzerland), Av: Avenches (Switzerland), Lo: London (England), Ma: Magdalensberg (Austria), Me: Menen (Belgium), Ni: Nijmegen (Netherlands), Ou: Oudenburg (Belgium), Ru: Rumst (Belgium), Tr: Trier (Germany).

<sup>b</sup> Vess: vessel, brac: bracelet, pend: pendant, ring: finger ring.

<sup>c</sup> All dates must be read as AD

Sample	Site <sup>a</sup>	Obj <sup>b</sup>	Cent <sup>c</sup>	Na <sub>2</sub> O	MgO	Al <sub>2</sub> O <sub>3</sub>	SiO <sub>2</sub>	P <sub>2</sub> O <sub>5</sub>	SO <sub>3</sub>	Cl	K <sub>2</sub> O	CaO	TiO <sub>2</sub>	MnO	Fe <sub>2</sub> O <sub>3</sub>	CuO	PbO
<b>High Magnesia Low Iron</b>																	
PC1_7	Ma	vess	I	16.2	3.3	2.5	64.0	0.5	nd	0.9	2.2	7.8	0.2	0.3	2.0	nd	nd
PC1_8	Ma	vess	I	19.6	1.9	1.9	66.1	nd	0.1	0.8	1.1	6.9	0.2	0.2	1.1	nd	nd
PC1_11	Ma	vess	I	20.0	1.5	2.7	65.5	nd	0.2	1.0	1.0	6.4	0.2	0.1	1.3	nd	nd
PC16_2	Lo	brac	I-II	20.3	4.5	1.6	65.5	nd	nd	1.1	2.4	3.3	0.3	nd	1.0	nd	nd
PC16_5	Lo	brac	I-II	20.9	5.2	2.3	63.4	nd	nd	0.8	1.9	3.7	0.3	nd	1.4	nd	nd
PC16_6	Lo	brac	I-II	20.4	4.4	4.2	60.6	nd	nd	0.7	3.3	3.9	0.4	nd	1.9	nd	nd
PC22_6	Av	vess	II-III	18.0	2.6	1.6	63.9	0.1	nd	0.9	1.9	8.6	0.1	0.5	1.6	nd	nd
PC22_7	Av	vess	II-III	17.2	2.9	1.8	63.0	nd	nd	0.9	1.6	10.4	0.1	0.4	1.5	nd	nd
PC22_12	Av	vess	II-III	15.3	3.3	1.6	63.4	0.1	nd	0.8	2.2	10.6	nd	0.4	2.2	nd	nd
PC23_2	Av	vess	II-III	15.1	3.3	1.6	63.7	nd	nd	0.7	2.4	10.3	0.1	0.4	2.1	nd	nd
PC23_3	Av	vess	II-III	19.2	2.1	2.9	62.6	nd	nd	1.1	1.2	8.5	0.3	0.3	1.6	0.1	nd
<b>Low Magnesia High Iron</b>																	
PC1_3	Ru	vess	II-III	16.5	0.6	1.8	66.4	nd	nd	0.7	0.7	6.2	nd	0.3	6.7	nd	nd
PC1_4	Ru	vess	II-III	17.0	0.5	1.6	63.9	nd	nd	0.9	0.6	5.5	nd	0.2	9.9	nd	nd
PC1_5	Ru	vess	II-III	16.7	0.5	1.7	65.9	nd	nd	0.7	0.7	6.2	nd	0.3	7.2	nd	nd
PC6_1	Au	vess	II-III	20.5	0.8	1.9	65.6	nd	nd	0.6	0.5	4.3	nd	0.2	5.6	nd	nd
PC6_2	Au	vess	II-III	20.8	0.8	2.0	65.9	nd	nd	0.6	0.5	4.3	nd	0.3	4.8	nd	nd
PC6_11	Au	brac	III-IV	19.3	0.5	1.8	65.2	nd	nd	0.7	0.6	5.9	nd	0.4	5.5	nd	nd
PC13_6	Tr	brac	III-IV	16.3	0.5	2.1	62.3	nd	nd	0.6	0.8	6.5	nd	0.3	10.5	nd	nd
PC13_8	Tr	brac	III-IV	16.6	0.6	2.0	63.9	nd	nd	0.6	0.7	6.3	nd	0.4	8.8	nd	nd
PC22_4	Av	vess	II-III	16.5	0.5	1.7	64.2	nd	nd	0.8	0.7	6.2	nd	0.2	9.0	0.1	nd
PC23_6	Me	ring	-	16.8	0.4	1.7	64.8	nd	nd	0.8	0.7	6.1	nd	0.2	8.3	nd	nd
PC23_8	Ni	vess	II-III	16.7	0.7	2.4	65.2	nd	nd	0.7	0.9	6.3	0.1	0.3	6.7	nd	nd
PC26_2	Ou	vess	III	16.5	0.7	1.7	64.4	nd	0.2	0.7	1.0	6.4	0.1	0.3	7.9	nd	nd
PC26_3	Ou	vess	III	16.6	0.8	1.7	65.2	nd	0.2	0.7	1.0	6.5	0.2	0.4	6.9	nd	nd
PC26_4	Ou	brac	III-IV	15.9	0.7	1.7	61.9	nd	0.2	0.6	1.0	6.0	0.1	0.3	11.5	nd	nd
<b>HIMT High Iron</b>																	
PC13_4	Tr	pend	IV-V	14.7	1.2	2.8	57.9	nd	nd	0.4	1.5	6.7	0.4	1.4	8.8	0.6	3.5
PC13_5	Tr	brac	IV-V	18.7	1.1	2.1	63.7	nd	nd	0.8	0.7	6	0.4	1.8	4.7	nd	nd

Table 2 XANES fitting parameters for all samples

Sample	Location	Position (eV)	Area	Total area	Width (eV)	Centroid (eV)	r <sup>2</sup>	Fe <sup>3+</sup> /ΣFe
<b>Reference compounds &amp; glasses</b>								
FeSO <sub>4</sub>		7111.68	0.0649	0.1323	2.1	7112.72	0.9996	0
		7113.2	0.0461					
		7114.82	0.0213					
ST1		7112.81	0.0821	0.2184	1.87	7113.77	0.9858	0.67
		7114.35	0.1363					
ST2		7112.58	0.073	0.2159	1.96	7113.67	0.9967	0.67
		7114.23	0.1429					
FeCl <sub>3</sub>		7112.9	0.0372	0.13	1.87	7114.1	0.999	1
		7114.14	0.0619					
		7115.45	0.0309					
<b>HMG: Low Iron</b>								
PC1.7	Magdalensberg	7112.29	0.0973	0.1863	2	7112.98	0.999	0.14
		7113.72	0.089					
PC1.8	Magdalensberg	7112.18	0.0914	0.1766	1.77	7112.91	0.9971	0.1
		7113.69	0.0852					
PC1.11	Magdalensberg	7112.37	0.104	0.1984	1.99	7113.1	0.9987	0.23
		7113.89	0.0944					
PC16.2	London	7112.39	0.0979	0.1706	1.67	7113.07	0.9964	0.21
		7113.98	0.0727					
PC16.5	London	7112.65	0.1194	0.2115	2.51	7113.2	0.9961	0.3
		7113.92	0.0921					
PC16.6	London	7112.23	0.0953	0.1957	1.98	7113.07	0.9949	0.21
		7113.85	0.1004					
PC22.6	Avenches	7112.32	0.0976	0.1964	1.99	7113.05	0.9991	0.19
		7113.77	0.0988					
PC22.7	Avenches	7112.32	0.1018	0.1837	1.92	7112.96	0.9988	0.13
		7113.76	0.0819					
PC22.12	Avenches	7112.22	0.1043	0.1903	2.01	7112.89	0.9991	0.08
		7113.71	0.086					
PC23.2	Avenches	7112.27	0.1003	0.1811	2.02	7112.89	0.9984	0.08
		7113.65	0.0808					
PC23.3	Avenches	7112.26	0.0926	0.182	1.77	7113	0.9989	0.16
		7113.78	0.0894					
<b>LMG: High Iron</b>								
PC1.3	Rumst	7112.26	0.1024	0.2108	1.95	7113.08	0.9991	0.22
		7113.85	0.1084					
PC1.4	Rumst	7112.31	0.1086	0.2242	2	7113.14	0.9992	0.26
		7113.92	0.1155					
PC1.5	Rumst	7112.42	0.1043	0.2149	1.98	7113.29	0.9994	0.36
		7114.11	0.1106					
PC6.1	Augst	7112.62	0.0997	0.2648	2.18	7113.68	0.9991	0.64
		7114.32	0.1652					
PC6.2	Augst	7112.59	0.0976	0.2502	2.11	7113.62	0.999	0.6
		7114.29	0.1526					
PC6.11	Augst	7112.39	0.0864	0.2312	2.09	7113.44	0.9986	0.47
		7114.07	0.1447					
PC13.6	Trier	7112.38	0.1021	0.2702	2.17	7113.42	0.9989	0.45
		7114.04	0.1682					
PC13.8	Trier	7112.51	0.0994	0.2617	2.07	7113.55	0.9991	0.55
		7114.18	0.1622					
PC22.4	Avenches	7112.56	0.1235	0.2529	2.09	7113.41	0.9994	0.45
		7114.21	0.1294					
PC23.6	Menen	7112.51	0.1262	0.2558	2.08	7113.36	0.9996	0.41
		7114.18	0.1296					
PC23.8	Nijmegen	7112.36	0.1238	0.235	2.01	7113.12	0.9995	0.24
		7113.96	0.1111					
PC26.2	Oudenburg	7112.39	0.106	0.2226	2.04	7113.28	0.9993	0.36
		7114.08	0.1166					
PC26.3	Oudenburg	7112.28	0.1001	0.1923	1.88	7113.04	0.9985	0.19
		7113.86	0.0922					
PC26.4	Oudenburg	7112.45	0.0945	0.2084	2.06	7113.35	0.9989	0.41
		7114.1	0.1139					
<b>HIMT: High Iron</b>								
PC13.4	Trier	7112.85	0.0781	0.3061	1.97	7113.91	0.9982	0.8
		7114.28	0.228					
PC13.5	Trier	7112.44	0.0924	0.2444	2.02	7113.48	0.999	0.5
		7114.11	0.1521					

1  
2  
3  
4  
5  
6  
7  
8  
9  
10  
11  
12  
13  
14  
15  
16  
17  
18  
19  
20  
21  
22  
23  
24  
25  
26  
27  
28  
29  
30  
31  
32  
33  
34  
35  
36  
37  
38  
39  
40  
41  
42  
43  
44  
45  
46  
47  
48  
49  
50  
51  
52  
53  
54  
55  
56  
57  
58  
59  
60

**IRON REDOX RATIO**

